Test of structural models for the (4 4) phase formed by oxygen adsorption on the Pt3Sn(1 1 1) surface

Available online at www.sciencedirect.com
SCIENCE DIRECT®
Surface Science 526 (2003) 193–200
SURFACE SCIENCE
www.elsevier.com/locate/susc

Test of structural models for the (4 × 4) phase formed by oxygen adsorption on the $Pt_3Sn(1\,1\,1)$ surface

A. Atrei [a,*], U. Bardi [b], G. Rovida [b], M. Torrini [b], M. Hoheisel [c], S. Speller [c]

[a] Dipartimento di Scienze e Tecnologie Chimiche e dei Biosistemi, Università di Siena, Via A. Moro, 53100 Siena, Italy
[b] Dipartimento di Chimica, Università di Firenze, Polo Scientifico di Sesto Fiorentino, Sesto Fiorentino (Firenze), Italy
[c] Research Institute for Materials, University of Nijmigen, 6525 ED Nijmigen, The Netherlands

Received 17 October 2002; accepted for publication 5 December 2002

Abstract

Exposure of the $Pt_3Sn(1\,1\,1)$ surface to oxygen at a pressure in the 10^{-6} mbar range at 800 K leads to the formation of a chemisorbed phase with a (4 × 4) periodicity. In previous works we investigated the structure of the (4 × 4) phase by means of scanning tunneling microscopy (STM) and XPD. STM images show that the (4 × 4) periodicity results from an array of protrusions and holes. XPD data suggest that oxygen adsorption induces the reconstruction of the substrate with the formation of a Sn–O overlayer. In the present work, several structural models compatible with the STM and XPD results were tested by tensor LEED analysis. The best agreement with the experimental *I–V* curves was obtained for a model similar to that proposed to interpret the STM images of the Ag(1 1 1)(4 × 4)–O phase. According to this structure, the protrusions observed in STM would correspond to tin atoms occupying on-top positions.

Keywords: Alloys; Platinum; Tin; Oxygen; Chemisorption; Surface structure, morphology, roughness, and topography; Low energy electron diffraction (LEED)

1. Introduction

The compositional and structural characterization of the phases formed upon oxygen exposure of Pt–Sn alloy surfaces is interesting from the point of view of the surface chemistry of this bimetallic system [1,2]. Surface alloys, prepared by evaporation of Sn on Pt(1 1 1) surface and subsequent annealing, [3–6] as well as the (1 1 1) surface of the Pt_3Sn alloy were used as substrates for oxygen adsorption [7]. The interaction of oxygen with Pt–Sn surface alloys has been investigated in details by means of X-ray photoelectron spectroscopy (XPS), Auger electron spectroscopy, thermal desorption spectroscopy, low-energy electron diffraction and scanning tunneling microscopy (STM) [3–6]. Depending on the oxidation conditions and the Sn concentration in the surface alloy, (5 × 5) and (4 × 4) LEED patterns were observed. The LEED patterns and the STM images were interpreted in terms of SnO_x clusters on the Pt(1 1 1) surface [3–6]. However, no information about the atomic structure of the features observed by STM was reported.

* Corresponding author. Tel.: +39-0577-234371; fax: +39-0577-234177.
E-mail address: atrei@unisi.it (A. Atrei).

0039-6028/02/$ - see front matter
doi:10.1016/S0039-6028(02)02650-X

A similar behavior is observed in the case of oxygen adsorption on $Pt_3Sn(1\,1\,1)$. XPS and low-energy ion scattering (LEIS) indicate that exposures at a pressure in the 10^{-6} mbar range at 800 K leads to saturation of the surface with a layer containing only oxygen and tin atoms [7]. The adsorbed phase formed under these conditions exhibits a sharp LEED pattern which can be indexed as a (4×4) superstructure with respect to the periodicity of the lattice of pure platinum only [8,9]. STM images of the (4×4) phase show the presence of an array of protrusions and holes. A typical STM image of the (4×4) structure is shown in Fig. 1. Similar images were observed upon oxygen exposure of the Pt–Sn surface alloys [6]. In order to get information about the nature of these protrusions we compared the experimental XPD intensities with single scattering cluster calculations performed for various structural models. On the basis of the analysis of the XPD results we could reduce the number of possible structural models and propose a tentative structure for the (4×4) phase. However, the XPD calculations did not allow us to distinguish among some of the structural models. In the present paper we report the results of a LEED intensity analysis of the (4×4) structure. The analysis of the diffracted intensities was carried out by means of the tensor LEED (TLEED) method [10,11]. A variety of models proposed on the basis of the XPD and STM results obtained in a previous work were tested as reference structures for the LEED calculations.

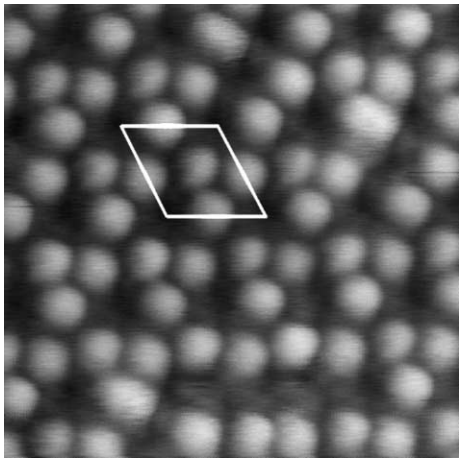

Fig. 1. Constant current STM image obtained for the $Pt_3Sn(1\,1\,1)(4 \times 4)$–O phase. Size: 5 nm × 5 nm. Tunneling current: 0.8 nA. Sample bias: 0.8 V. The zigzag displacement of the protrusions is visible in the image. The (4×4) unit cell is shown.

2. Experimental and calculation procedure

2.1. Experimental

The experiments were carried out in a ultra-high vacuum chamber equipped with ion gun, X-ray source and hemispherical analyzer for sample preparation and characterization. The LEED measurements were performed by means of a three-grid rear view LEED optics. The intensities versus accelerating voltage (I–V) curves of the diffracted beams were collected using a video LEED system. The $Pt_3Sn(1\,1\,1)$ sample was the same used in previous studies and was prepared as described in Ref. [8]. The surface was prepared by cycles of argon ion sputtering (1 keV) and annealing (up to 1000 K for 30 min) until no contamination was detectable by means of XPS and LEIS and the (2×2) LEED pattern characteristic of the clean surface was observed [8,9]. The (4×4) structure was prepared by exposing the sample to O_2 (at a pressure of 1×10^{-6} mbar) with the sample held at 800 K. Under these conditions oxygen uptake is a self-limiting process leading to the formation of the (4×4) phase. Details about the characterization of the growth mechanism and composition of the (4×4) phase are presented in Ref. [7]. The LEED I–V curves were measured at normal incidence of the electron beam in the energy range 20–300 eV. Normal incidence was considered to be achieved when reliability factors (Pendry R-factor [12]) between I–V curves of symmetrically equivalent beams of 0.1 or below were obtained. The I–V curves of symmetric beams were averaged to compensate for minor differences due to small deviations from normal incidence. The I–V curves were background subtracted and normalized to constant incident electron current. The LEED intensities were collected at room temperature.

STM measurements were performed in an other experimental chamber equipped with an Omicron microscope [7].

2.2. TLEED calculations

The TLEED method consists of a first step in which a full dynamical calculation is performed for a chosen reference structure to produce the elements of the tensor. With this tensor, the *I–V* curves for a variety of models close to the reference structure can be fastly calculated, using a perturbation method [10].

The TLEED calculations were performed by means of the Barbieri/Van Hove Symmetrized Automated Tensor LEED package (SATLEED) [11]. The Barbieri–Van Hove program package was used for the calculation of the phase shifts [11]. Ten phase shifts ($l_{max} = 9$) were used in the LEED calculations. The phase shifts for platinum and tin were calculated from a muffin–tin potential of Pt_3Sn. The oxygen phase shifts were derived from a muffin–tin potential of SnO_2. Another set of oxygen phase shifts were calculated from the muffin–tin potential of an oxygen overlayer on the $Pt_3Sn(1\,1\,1)$ surface (to avoid problems with different values of the inner potential of SnO_2 and Pt_3Sn). Test LEED calculations performed with the two sets of phase shifts lead to results which do not differ significantly. The LEED calculations were performed between 20 and 200 eV. The imaginary part of inner potential was set to 5 eV, whereas the real part was set to 10 eV and optimized in the search procedure. The Debye temperatures were initially set to 300, 300 and 500 K for platinum, tin and oxygen respectively [8,13] and refined in the optimization process. In the automated search of the structural parameters giving the best agreement with the experimental *I–V* curves nine non-equivalent beams were used for a total energy range of about 900 eV. The Pendry reliability factor (R_p), was used in the analysis to judge the agreement between experimental and calculated *I–V* curves [12]. Since the *I–V* curves were collected at normal incidence they are more sensitive to the interlayer spacings than to the in-plane atomic positions. Hence, in a first step of the analysis, only the coordinates perpendicular to the surface were allowed to vary. Then, starting from the optimized values of these coordinates, also the atomic positions parallel to the surface were optimized. Whenever the displacements from the atomic positions in the reference structure were larger than 0.2–0.3 Å, calculations for a new reference structure (starting from the previously optimized coordinates) were performed.

3. Results and discussions

The first structural model tested in the TLEED analysis is shown in Fig. 2. Model 1 was proposed on the basis of the XPD results [7]. The arrangement of Sn atoms in the overlayer is similar to that in the (1 0 1) plane of SnO. One side of the unit of SnO(1 0 1) is equal to the Sn–Sn first nearest neighbor distance in the overlayer (3.77 Å) [7]. This produces a (4×4) coincidence net with the periodicity of the substrate. The holes observed in STM would correspond to the missing Sn atoms occupying on-top positions. The protrusions seen by STM can be attributed to groups of tin atoms, each group consisting of two atoms close to bridge positions on the substrate surface. The composition of the overlayer is Sn_8O_6. For the reference

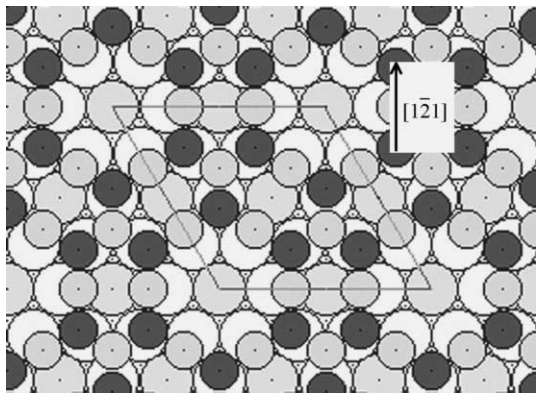

Fig. 2. Model 1 for the $Pt_3Sn(1\,1\,1)(4 \times 4)$–O phase. Dark circles: oxygen atoms, smaller grey circles: tin atoms in the overlayer, larger grey circles: tin atoms in the substrate, white circles: platinum atoms. The periodicity of the overlayer is referred to that of the substrate containing only Pt. The (4×4) unit cell is drawn on the structure. The [1 $\bar{2}$ 1] direction is indicated in the figure.

structure calculations, the oxygen–tin and the overlayer–substrate interlayer distances were 1.00 and 2.30 Å, respectively. These values were obtained from the analysis of the XPD data [7]. Atoms in the topmost layer of the substrate were kept at the bulk positions and only the coordinates of atoms in the overlayer were optimized. Also the composition of the outermost layer of the substrate was kept to the bulk value. The I–V curves calculated for model 1 gave a very poor agreement with the experimental data as indicated by the value of R_p (0.64). Hence, the coincidence net model shown in Fig. 2 can be ruled out.

The other structural models tested in this work are shown in Figs. 3–5. These models differ for the positions (and number) of oxygen atoms. The composition is $Sn_{11}O_{12}$ for models 2 and 4 and $Sn_{11}O_9$ for model 3. In all structures, some of the tin atoms occupy on-top positions with respect to the substrate atoms. In alternate rows, one every two of these atoms is missing to produce the (4×4) periodicity. According to this structure, the bright features seen by STM would correspond to on-top tin atoms, whereas the missing of such atoms would produce the holes. As far as the positions of Sn atoms are concerned, this structure is similar to that proposed to interpret the STM images of the Ag(1 1 1)(4×4)–O phase [14]. Simulations of the STM images performed for such structures indicate that the bright features correspond to metal atoms occupying on-top positions [14]. The positions of oxygen atoms were chosen in order to be consistent with the XPD results [7]. That is, in such a way that the peaks due to photoelectrons emitted by Sn atoms in the overlayer and scattered by oxygen atoms are in the same azimuthal directions as in the experimental XPD pattern. In the reference structures the O–Sn interlayer distances were calculated assuming a O–Sn first-nearest neighbor distance of 2.0 Å [7]. Because of the zigzag displacements of the pro-

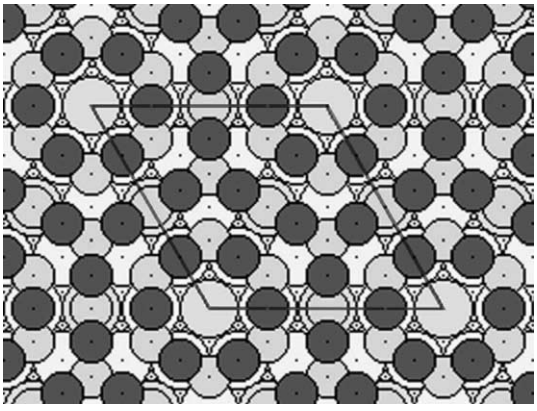

Fig. 3. Model 2. The structure of tin atoms in the overlayer is similar to that of silver atoms in the Ag(1 1 1)(4×4)–O phase. Oxygen atoms occupy bridge positions on the Sn atoms in the overlayer.

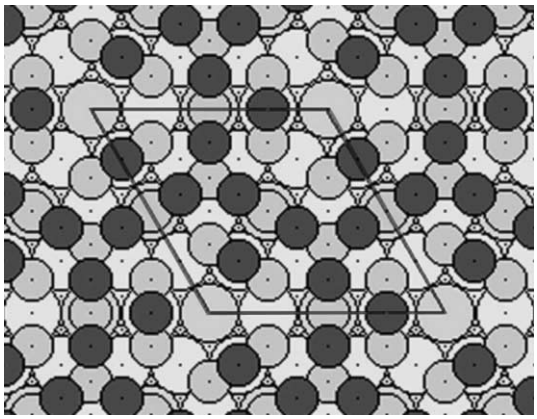

Fig. 4. Model 3. The positions of tin and oxygen atoms are the same as those in model 2. One oxygen atom around each on-top Sn atom is missing.

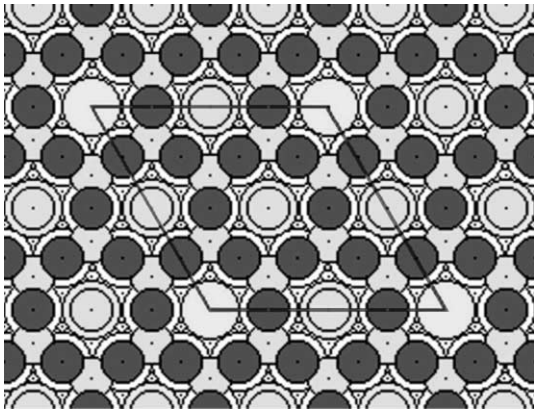

Fig. 5. Model 4. As far as the positions of tin atoms are concerned the structure is the same of model 2, but the positions of oxygen atoms are different.

trusions observed in STM (Fig. 1) the surface has three-fold rotational axes (3P two-dimensional space group). On the other hand the substrate has mirror planes (along the $[1\,\bar{2}\,1]$ and equivalent directions) in addition to the three-fold rotational axis. This implies the existence of domains produced by the mirror planes of the substrate. To take into account the existence of domains, the proper calculated I–V curves were averaged prior to the comparison with the experimental curves.

Even limiting the analysis to the optimization of the coordinates perpendicular to the surface, models 2, 3 and 4 gave an R-factor lower than model 1. This result suggests that the positions of Sn atoms are substantially correct. In the following of the analysis we optimized the in-plane coordinates of the atoms. Because of the large number of parameters to be fitted (as large as 24) the optimization procedure is a critical task. First of all, the fitting procedure may lead to local minima of the R-factor in the parameter space. Moreover, the analysis can bring to a minimum of the R-factor which corresponds to unphysical results (like too short bond lengths). This can occur for parameters which affect scarcely the I–V curves (e.g. the in-plane oxygen coordinates). The parameters are varied in the searching procedure reaching meaningless values to decrease the R-factor.

The optimization of the in-plane atomic positions for model 2 and model 3 leaded to a decrease of R_p which, however, did not go below 0.5 (see Table 1). On the other hand, R_p dropped substantially after optimization of the in-plane coordinates for model 4. For this model, we performed reference structure calculations on a grid of values (from 0.20 to 1.00 Å, with a step of 0.20 Å) of the lateral displacement of Sn atoms from the on-top positions (Fig. 6). The remaining Sn atoms were kept fixed in the three-fold hollow sites of the substrate. Also the in-plane coordinates of oxygen atoms were not varied ($\delta_{O1} = \delta_{O2} = \delta_{O3} = 0.00$ Å). For each of these reference structures the coordinates perpendicular to the surface were optimized. With these constrains the best fit was obtained for $\delta_{Sn} = 0.80$ Å (see Fig. 7). For each value of δ_{Sn}, we performed reference structure calculations for lateral displacements of oxygen atoms in the directions indicated in Fig. 6a and b. In a first step, equal values of δ_{O1}, δ_{O2} and δ_{O3} were considered.

Table 1
Minimum values of the Pendry R-factor (R_p) obtained for the basic structural models tested in the TLEED analysis

Model no.	R_p
1	0.70 (a), 0.60 (b)
2	0.59 (a), 0.51 (b)
3	0.58 (a), 0.50 (b)
4	0.53 (a), 0.39 (b)

R_p obtained optimizing the atomic coordinates perpendicular to the surface only (a) and the atomic coordinates perpendicular and parallel to the surface (b).

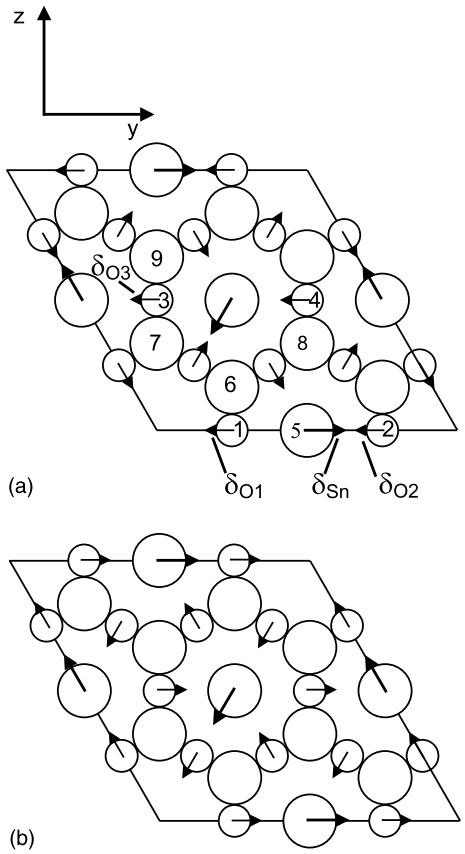

Fig. 6. Schematic representation of model 4. Large circles: tin atoms, small circles: oxygen atoms. The arrows indicate the lateral displacements of tin and oxygen atoms. Negative values of δ indicate displacements towards the negative direction of the y-axis. (a) $\delta_{Sn} > 0$, $\delta_{O1} = \delta_{O2} = \delta_{O3} < 0$. (b) $\delta_{Sn} > 0$, $\delta_{O1} = \delta_{O2} = \delta_{O3} > 0$. The symmetry equivalent domain is obtained by applying the mirror plane of the substrate along the $y = 0$ direction.

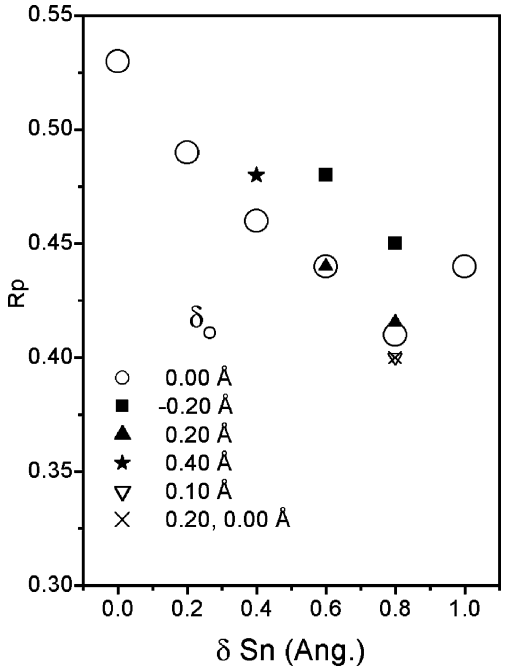

Fig. 7. R_p as a function of the lateral displacements of Sn atoms from the on-top position. The values of δ_O were fixed at the values reported in the figure whereas the x-coordinates were optimized in the search of the best-fit. For the point indicated by a cross, $\delta = \delta_{O1} = \delta_{O2} = 0.20$ Å and $\delta_{O3} = 0.00$ Å.

These calculations allows us to put an upper limit of 0.20 Å to the δ_O values since above this limit the agreement with the experimental data gets significantly worst. For $\delta_{Sn} = 0.8$ Å, reference structure calculations were carried out for $\delta_{O1} = \delta_{O2} = 0.20$ Å and $\delta_{O3} = 0.00$ Å and for $\delta_{O1} = \delta_{O3} = 0.20$ Å and $\delta_{O2} = 0.00$ Å. The refinement of the lateral displacements of oxygen atoms in the directions shown in Fig. 6b leads to a minimum of $R_p = 0.39$ which was obtained for $\delta_{O1} = \delta_{O2} = \delta_{O3} = 0.10$ Å. When all the parameters were free to vary the automatic search of the best fit leaded to an R-factors of 0.35. However, this minimum of the R-factor has to be considered an artefact since it corresponds to too short O–Sn bond lengths. The decrease of the R-factor is probably due to the increased number of fitting parameters. A test, based on the number of structural parameters and number of experimental data (for LEED the total energy range of the I–V curves), confirms this interpretation [15].

As a further step of the analysis, the possibility to vary the atomic positions and composition in the first layer of the alloy was included in the calculations. The sensitivity of the LEED intensities to the positions of the atoms in the outermost layer of the alloy is rather low and the buckling of this layer is within the error bar of this analysis. The effect of the composition of the substrate outermost layer on the LEED intensities is also weak. However, a slight increase of the R-factor is obtained when considering a substrate of pure platinum. Calculations performed for various values of the Debye temperatures of oxygen and tin and imaginary part of the inner potential indicate that the agreement is not influenced significantly by these non-structural parameters. The structural parameters corresponding to the optimized structure are reported in Table 2 and the comparison of the calculated and experimental I–V curves is shown in Fig. 8. In the optimized structure there are O–Sn bond lengths ranging from 1.92 to 2.18 Å whereas the interlayer spacing between the substrate and the overlayer (the vertical distance between the atoms in the outermost layer of the substrate and the deepest atom in the overlayer) is 2.37 ± 0.10 Å. The level of agreement between

Table 2
Parameters corresponding to the best-fit structure

Atom no.	Element	x (Å)	Δx (Å)	δ (Å)
1	O	0.00	−0.09	0.10
2	O	0.00	−0.09	0.10
3	O	0.00	−0.34	0.10
4	O	0.00	−0.19	0.10
5	Sn	0.50	−0.07	0.80
6	Sn	1.00	−0.07	–
7	Sn	1.00	−0.09	–
8	Sn	1.00	−0.19	–
9	Sn	1.00	−0.35	–

Atoms are numbered referring to Fig. 6. x are the coordinates of the atoms perpendicular to the surface in the reference structure. The positive direction of the x-axis is towards the crystal. Δx are the displacements perpendicular to the surface with respect to the values in the starting reference structure in Fig. 5. δ are the lateral displacements of tin and oxygen atoms from the reference structure in the directions shown in Fig. 6b. The error bars are estimated to be ± 0.10 and ± 0.20 Å for the x-coordinates and the lateral displacements, respectively from the variance of Pendry R-factor [12].

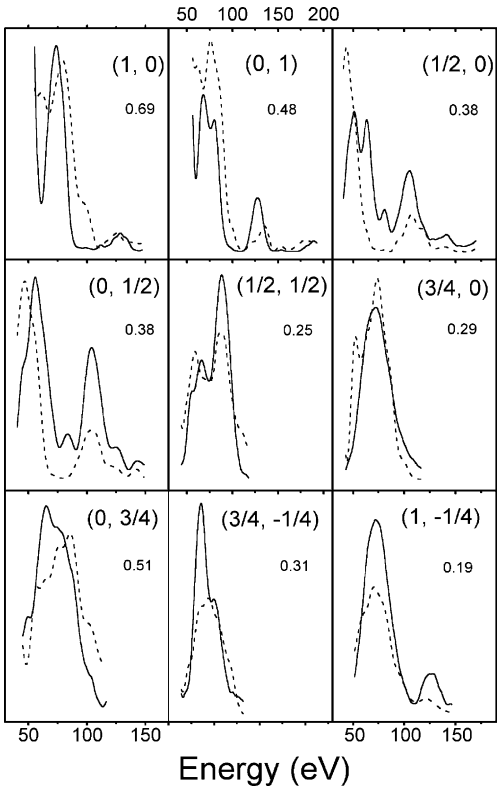

Fig. 8. Comparison of experimental (solid line) and calculated for the best fit model (dashed line) I–V curves. For each beam the value of R_p is reported.

calculated and experimental I–V curves appears to be acceptable considering the complexity of the structure. The moderate level of agreement can be explained considering the difficulties in determining the real minimum with such a large number of parameters to be fitted. In order to improve the search of the best-fit structure, resulting in a more accurate determination of the structural parameters, a larger experimental data set would be needed. For a significant increase of the total energy range, the I–V curves should be collected at low temperature.

Nonetheless, the LEED analysis provides an evidence for a zigzag displacement of Sn atoms in the overlayer. The amplitude of such displacement is consistent with the lateral displacement of the protrusions from the rows of holes (≈0.5 Å) observed by STM. In the unrelaxed structure of Fig. 5 each on-top Sn atom is surrounded by six oxygen atoms at 2.87 Å. With the lateral displacements determined by LEED, each Sn atom get closer to an oxygen atom (interatomic distance of 2.18 ± 0.20 Å). The formation of such Sn–O bond could be the driving force for such movements.

4. Conclusions

The TLEED analysis of the $Pt_3Sn(1\,1\,1)(4 \times 4)$–O phase allowed us to rule to out possible models proposed on the basis of previous STM and XPD results. Amongst the structures tested in the LEED calculations only one model gives an acceptable level of agreement. According to this structure, the ordered array of protrusions observed by STM would corresponds to Sn atoms sitting close to on-top positions on the substrate surface whereas the missing of such Sn atoms would give rise to the holes. The zigzag of the protrusions seen by STM would be produced by displacement of tin atoms from the on-top positions.

Acknowledgements

This work was supported by MURST under the program "Crescita, struttura e reattività di superfici di materiali e film metallici" COFIN2000.

References

[1] A. Haner, P.N. Ross, U. Bardi, Catal. Lett. 8 (1991) 1.
[2] K. Wang, H. Gasteiger, N. Markovic, P.N. Ross, Electrochim. Acta 41 (1996) 2587.
[3] M. Batzill, D.E. Beck, B.E. Koel, Appl. Phys. Lett. 78 (2001) 2766.
[4] M. Batzill, D.E. Beck, D. Jerdev, B.E. Koel, J. Vac. Sci. Technol. A 19 (2001) 1953.
[5] D. Jerdev, B. Koel, Surf. Sci. 492 (2001) 106.
[6] M. Batzill, D.E. Beck, B.E. Koel, Phys. Rev. B 64 (2001) 245402.
[7] M. Hoheisel, W. Heiland, S. Speller, A. Atrei, U. Bardi, G. Rovida, Phys. Rev. B 66 (2002) 165416.
[8] A. Atrei, U. Bardi, G. Rovida, M. Torrini, E. Zanazzi, Phys. Rev. B 46 (1992) 1649.
[9] J. Kuntze, S. Speller, W. Heiland, I. Spolveri, U. Bardi, Phys. Rev. B 58 (1998) 16005.

[10] M.A. Van Hove, W. Moritz, H. Over, P.J. Rous, A. Wander, A. Barbieri, M. Materer, U. Starke, G.A. Somorjai, Surf. Sci. Rep. 19 (1993) 191.
[11] A. Barbieri, M.A. Van Hove, Symmetrized Automated Tensor LEED Package. Available from: <http://www.lbl.gov.software>.
[12] M.A. Van Hove, W.H. Weinberg, C.-M. Chan, Low-energy Electron Diffraction: Experiment, Theory and Structural Determination, Springer Series in Surface Science, vol. 6, Springer, Berlin, 1986.
[13] A. Atrei, E. Zanazzi, U. Bardi, G. Rovida, Surf. Sci. 475 (2001) L223.
[14] C.I. Carlisle, D.A. King, M.-L. Bocquet, J. Cerdá, P. Sautet, Phys. Rev. Lett. 84 (2000) 3899.
[15] C.F. Walters, K.F. Mc Carty, E.A. Soares, M.A. Van Hove, Surf. Sci. 464 (2000) L732.